Octahedral Coordination at the High-Affinity Metal Site in Enolase: Crystallographic Analysis of the Mg^{II}−Enzyme Complex from Yeast at 1.9 Å Resolution†

Joseph E. Wedekind, George H. Reed,* and Ivan Rayment*

Institute for Enzyme Research, Graduate School, and Department of Biochemistry, College of Agricultural and Life Sciences, University of Wisconsin−Madison, Madison, Wisconsin 53705

Received November 18, 1994; Revised Manuscript Received January 10, 1995®

ABSTRACT: The structure of the Mg^{2+} complex of yeast enolase has been determined from crystals grown in solutions of poly(ethylene glycol) at pH 8.1. Crystals belong to the space group $P2_1$ and have unit cell dimensions $a = 72.5$ Å, $b = 73.2$ Å, $c = 89.1$ Å, and $\beta = 104.4°$. There is one dimer in the asymmetric unit. The current crystallographic *R*-factor is 19.0% for all recorded data to 1.9 Å resolution. The electron density indicates a hexacoordinate Mg^{2+} at the high-affinity cation binding site. The octahedral coordination sphere consists of a meridional arrangement of three carboxylate oxygens from the side chains of Asp 246, Asp 320, and Glu 295, and three well-ordered water molecules. Octahedral coordination is the preferred geometry for alkaline earth metal ions in complexes with oxygen donor groups. In previous crystallographic studies of enolase, Zn^{2+} and Mg^{2+} complexes at the high-affinity site were reported to exist in trigonal bipyramidal coordination. This geometry was suggested to enhance the electrophilicity of the metal ion and promote rapid ligand exchange [Lebioda, L., & Stec, B. (1989) *J. Am. Chem. Soc. 111,* 8511−8513]. The octahedral arrangement of carboxylate and water ligands in the Mg^{II}-enolase complex determined here is most consistent with reports of the Mn^{2+} and Mg^{2+} coordination complexes of mandelate racemase and muconate lactonizing enzyme. These latter enzymes have α/β-barrel folds comparable to enolase. Furthermore, coordination to Mg^{2+} in the present study is compatible with the geometry observed in the enolase−$(Mg^{II})_2$−phosphonoacetohydroxamate structure [Wedekind, J. E., Poyner, R. R., Reed, G. H., & Rayment, I. (1994) *Biochemistry 33,* 9333−9342]. In the latter structure, oxygen atoms from the hydroxamate and carbonyl groups of the inhibitor displace two of the three water ligands in the Mg^{II}-enolase coordination sphere. Conservation of metal ligand geometry between the inhibited and the noninhibited enzyme and the observation of hexacoordination in other α/β−barrel enzymes suggest octahedral geometry is the relevant coordination state of the high-affinity metal in enolase.

Enolase catalyzes the reversible dehydration of 2-phospho-D-glycerate (2-PGA)[1] in the glycolytic pathway. Two equivalents of divalent cation are required per subunit to elicit full activity (Faller et al., 1977). This requirement is met most effectively by Mg^{2+}, Mn^{2+}, or Zn^{2+} (Wold & Ballou, 1957). The metals bind to enolase in a sequential manner with different affinities. The higher affinity metal site[2] (metal **I**) is occupied first in the apo-enzyme. Coordination at this site is difficult to eliminate without the use of high chelator concentrations. The second metal ion (metal **II**) interacts synergistically with substrate such that it is the third component to bind in the M^{II}−substrate−M^{II} precatalytic complex (Anderson, 1981). Previous crystallographic studies of Zn^{II}−enolase showed what appeared to be trigonal bipyramidal geometry at site **I**. This geometry was postulated to account for the high degree of polarization required to generate the carbanion intermediate and to facilitate rapid ligand exchange (Lebioda & Stec, 1989). Although the structure of Mg^{II}-enolase was not reported, continued support for pentacoordination at site **I** appeared in structures of the Mg^{II}−enolase−2-PGA/PEP, Zn^{II}−enolase−PG, and Mg^{II}−enolase−F^-−P_i complexes (Lebioda & Stec, 1991; Lebioda et al., 1991, 1993). One exception was the inactive Ca^{II}−2-PGA−enolase complex which showed octahedral coordination geometry at site **I** (Lebioda et al., 1991). Three of these structures were reported at higher than 2.2 Å resolution, which is sufficient for the assignment of waters in the metal coordination sphere. Such earlier crystallographic studies were obtained from a single crystal form (Lebioda & Brewer, 1984) into which various components were added through soaking in a synthetic mother liquor of 3 M $(NH_4)_2SO_4$ at pH 6.0. Under these conditions, the enzyme displays approximately 5% of the maximum velocity achieved in an ionic strength of 0.05 M at pH 7.8 (Lebioda et al., 1989). Optimum enzyme activity occurs at pH 7.7 for the yeast enzyme (Cardenas & Wold, 1971).

† This research was supported in part by NIH grants GM35752 (G.H.R.), GM39082, and AR35186 (I.R.) and by an NRSA Fellowship (J.E.W.) from NIH Training Grant GM08293.

* Address correspondence to these authors at the Institute for Enzyme Research, University of Wisconsin, 1710 University Ave., Madison, WI 53705. FAX: 608-265-2904.

® Abstract published in *Advance ACS Abstracts,* March 1, 1995.

[1] Abbreviations: 2-PGA, 2-phospho-D-glycerate; PEP, phosphoenolpyruvate; M^{II}, divalent metal ion; PG, phosphoglycolate; PhAH, phosphonoacetohydroxamate; PDB, Brookhaven Protein Data Bank; MR, mandelate racemase; CMLE, chloromuconate lactonizing enzyme; MLE, muconate lactonizing enzyme; PEG, poly(ethylene glycol); rms, root-mean-square; HEPPS, *N*-(2-hydroxyethyl)piperazine-*N*′-3-propanesulfonic acid.

[2] The metal ion which binds tightly to enolase in the absence of substrates has been called the "conformational" metal. The second metal ion which binds in the presence of substrate has been called the "catalytic" metal. Because both metals are essential for catalysis, we refer to the two divalent cations in order of decreasing binding affinity as metal **I** and metal **II**, respectively.

0006-2960/95/0434-4325$09.00/0

Table 1: Intensity Statistics for the Native X-ray Data Set

		shell (Å)								
	total	100−5.69	−4.03	−3.29	−2.85	−2.55	−2.33	−2.15	−2.02	−1.90
observations	77897	4570	9279	11579	13152	13008	6989	6553	6375	6392
total independent reflections[a]	53410	2697 (1873)	4874 (4405)	6211 (5368)	7198 (5954)	7669 (5339)	6287 (702)	6165 (388)	6115 (260)	6194 (198)
theoretical (%)	75	98	100	99	97	92	69	59	61	54
intensity (av)		2257	2587	1933	968	578	510	409	258	129
σ		65	97	90	65	58	59	59	59	52
R-factor[b] (%)	4.1	1.8	2.4	3.1	4.7	7.0	8.9	11.2	17.5	29.0

[a] The number of reduced observations. In parentheses is the number of independent measurements for which there were duplicate or symmetry-related observations. [b] R-factor = $(\sum|I - \bar{I}|/\sum I) \times 100$.

More recently, the tight binding inhibitor PhAH was crystallized as a complex with enolase from PEG at pH 8.2, revealing hexacoordinate Mg^{2+} geometry at both site **I** and site **II** (Wedekind et al., 1994). The corresponding Mn^{2+} complex of enolase and PhAH, obtained by soaking the low-pH high-salt crystals in solutions of the inhibitor (Zhang et al., 1994), also revealed a hexacoordinate Mn^{2+} at site **I**, although the electron density was not well-defined for the second Mn^{2+} binding site (Zhang et al., 1994). The latter study attributed the octahedral geometry of Mn^{2+} at site **I** to the unusual properties of the inhibitor (Zhang et al., 1994). Thus, the possibility remained that an atypical trigonal bipyramidal coordination at site **I** could confer a mechanistically important advantage in the enolase reaction.

The molecular structures of three other divalent cation-dependent, α/β-barrel enzymes are known—chloromuconate lactonizing enzyme (Hoier et al., 1994), muconate lactonizing enzyme (Goldman et al., 1987), and mandelate racemase (Neidhart et al., 1991). Crystal structures of MR and MLE have been refined beyond 1.9 Å resolution (PDB entry 2MNR; Hoier et al., 1994). Interestingly, the substrate- and inhibitor-free forms of these enzymes revealed octahedral coordination at their respective metal binding sites which are structurally equivalent to site **I** of enolase. In order to clarify the coordination geometry for Mg^{2+} at site **I** of enolase, the high-resolution structure of the Mg^{II}—enolase complex was obtained from crystals grown in PEG at pH 8.1 and compared to the divalent metal ion coordination schemes in other α/β-barrel enzymes, described below. This work complements the earlier structural study of the enzyme complexed with Mg^{2+} and the inhibitor, PhAH (Wedekind et al., 1994).

EXPERIMENTAL PROCEDURES

Structure Determination. Enolase was purified, crystallized, and characterized as reported previously (Wedekind et al., 1994). Crystals were grown by batch from 16% (w/w) PEG 8000, 0.25 M KCl, 0.04 M HEPPS buffer, pH 8.0, and 0.5 mM $MgCl_2$. X-ray data were recorded at 4 °C with a Siemens X-1000D multiwire area detector at a crystal-to-detector distance of 12 cm. Ni-filtered CuKα radiation was from a Rigaku RU 200 rotating anode X-ray generator with a 200 μm focal spot, operated at 50 kV × 50 mA. Diffraction data from three crystals were processed with the XDS data reduction software of Kabsch (1988a,b), and scaled by the method of Fox and Holmes (1966). The data set was 75% complete to 1.9 Å resolution with an overall merging R-factor of 4.1% (Table 1).

Molecular Replacement. The Mg^{II}-enolase complex was solved by molecular replacement with the AMORE software programs of Navaza (1987, 1990). Coordinates of dimeric apo-enolase (Stec & Lebioda, 1990) were used as the search model. A cross-rotation function, calculated from X-ray data between 4.0 and 8 Å resolution, generated four peaks of equal height related by 180°. A single solution was chosen having Euler angles $\alpha = 173.3°$, $\beta = 106.5°$, and $\gamma = 323.5°$. The location of one dimer was determined by the corresponding translation function which had a translational component in fractional coordinates of $a = 0.125$, $b = 0.358$, and $c = 0.692$. Rigid body refinement (Castellano et al., 1992) using data between 20 and 3.5 Å resolution resulted in an initial crystallographic R-factor of 37% for all measured data to 2.7 Å resolution.

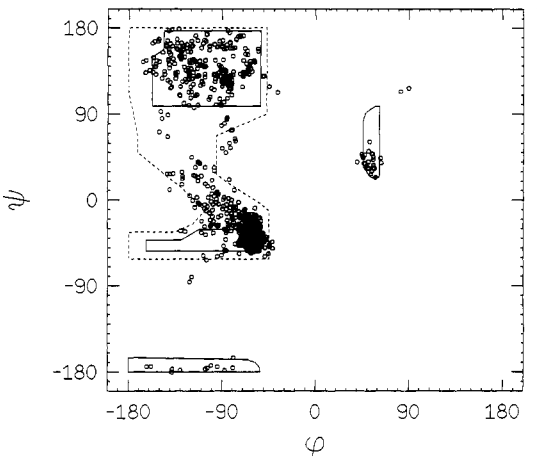

FIGURE 1: Ramachandran plot of dimeric yeast enolase main-chain non-glycinyl dihedral angles. Fully allowed φ, ψ values are shown by solid enclosures. Partially allowed regions are enclosed by dashed lines. Dihedral angles of most residues outside the allowed regions can be accounted for by hydrogen bonding and ionic interactions. For example, Arg 402 is the left-handed helical outlier whose guanidinium group interacts with Glu 404. A carboxylate oxygen atom of Asp 320 interacts with Mg^{2+}, causing a right-handed helical distortion ($\varphi = -120$, $\psi = -80$).

Refinement. Crystallographic least-squares refinement of the preliminary model by the program TNT (Tronrud, 1987) followed by simulated annealing with XPLOR (Brünger, 1992) reduced the R-factor to 24% for all data to 2.4 Å resolution. Electron density maps with the coefficients $2F_o - F_c$ and $F_o - F_c$ were used in manual rebuilding with the program FRODO (Jones, 1978). Manual fitting and addition of 2 Mg^{2+} ions and 126 water molecules (CCP4, 1979) were performed prior to least-squares refinement with all data to 1.9 Å resolution. Additional waters were included with the interactive graphics program CHAIN (Sack, 1988). Waters were included only when they appeared in both $2F_o - F_c$ and $F_o - F_c$ maps at contour levels greater than 1σ and when they were within 3.6 Å of a hydrogen bonding partner.

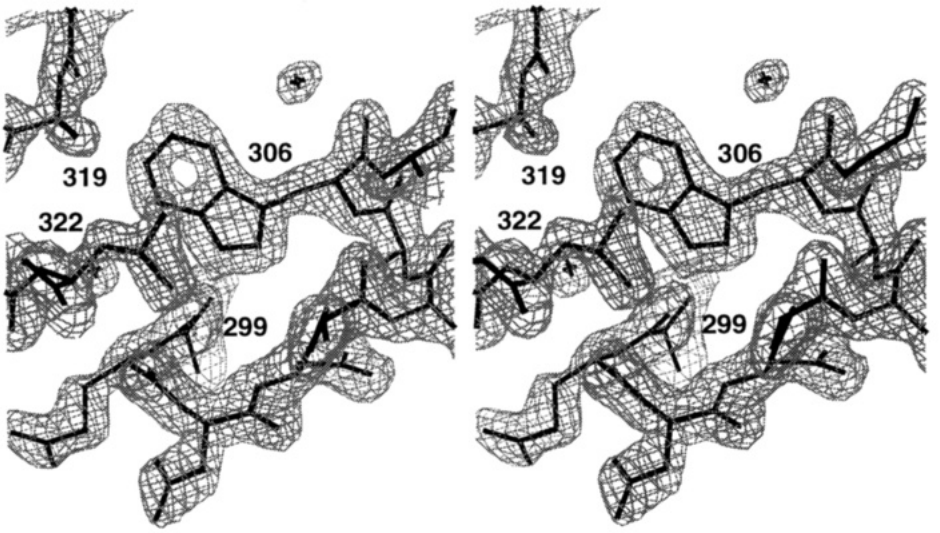

FIGURE 2: Representative $2F_o-F_c$ electron density contoured at 1.2σ (subunit II). A loop and a helix extending from Ala 299 through Ser 307 are shown. Ala 319, Leu 322, and Trp 306 form a hydrophobic pocket. The NE1 hydrogen of the Trp 306 indole ring projects toward the carbonyl oxygen of Ala 299. Two representative solvent molecules are shown. Figures 2 and 4 were generated by FROST (G. Wesenberg, University of Wisconsin).

Chloride ions (average $B = 34$ Å^2) were assigned to two large density peaks ($>5\sigma$) located at the phosphate binding site (Stec & Lebioda, 1990; Lebioda & Stec, 1991) in each respective subunit. Additional nonsolvent electron density originating at Ser 36 was modeled in the closed conformation of the active site loop. Atom occupancies for both open and closed conformations totaled unity. Initial partial occupancies were set at 0.5, and were later adjusted according to the results of correlated *B*-factor refinement. The current *R*-factor for all data recorded to 1.9 Å resolution is 19.0%. The present dimeric model includes 507 water molecules (temperature factors ≤93 Å^2). The root-mean-square deviations from ideal geometry are 0.019 Å for bond lengths, 2.2° for bond angles, and 0.007 Å for coplanar groups. A Ramachandran plot for the dimer main-chain non-glycinyl dihedral angles is shown in Figure 1.

RESULTS AND DISCUSSION

Enolase from baker's yeast is a dimer of chemically identical subunits (referred to as I and II, designated as chains *A* and *B*). Each subunit consists of 436 amino acids comprising 2 domains (Stec & Lebioda, 1990). Representative electron density for the refined Mg^{II}-enolase complex obtained from crystals grown in PEG at pH 8.1 is shown in Figure 2. A comparison to several other enolase structures reveals close similarities in the positions of α carbons. In particular, the Mg^{II}-enolase complex superimposes well with the dimeric forms of the apo, Zn^{II}−holo, Ca^{II}−2-PGA, and Mg^{II}−PG enolase structures obtained from high salt and low pH (Stec & Lebioda, 1990; Lebioda & Stec, 1989; Lebioda et al., 1991); the average rms deviation of these four structures from the Mg^{II}-enolase complex is 0.40 Å. Superpositions were obtained by the algorithm of Kabsch (1978). Subtle differences evident in a comparison of the low-salt Mg^{II}-enolase structure to previous high-salt structures include the presence of a *trans* proline at residue 265 and the existence of electron density for both the open and closed conformations of the active site loop. Subunit I, residues Val 34 through Ala 38, was assigned partial occupancies ranging from 0.5 to 0.8 to reflect the open conformation; residues Pro 35 through Ala 38 of subunit II were assigned similar occupancies. Electron density corresponding to the side chain of Thr 40 was present in the closed conformation, but was modeled as solvent in both subunits due to the absence of well-defined main-chain electron density for residues 39−42. The model for the open conformation of Mg^{II}-enolase, extending from residues 35 to 42, resembles that described previously (Stec & Lebioda, 1990). Although the active site loop has been reported in

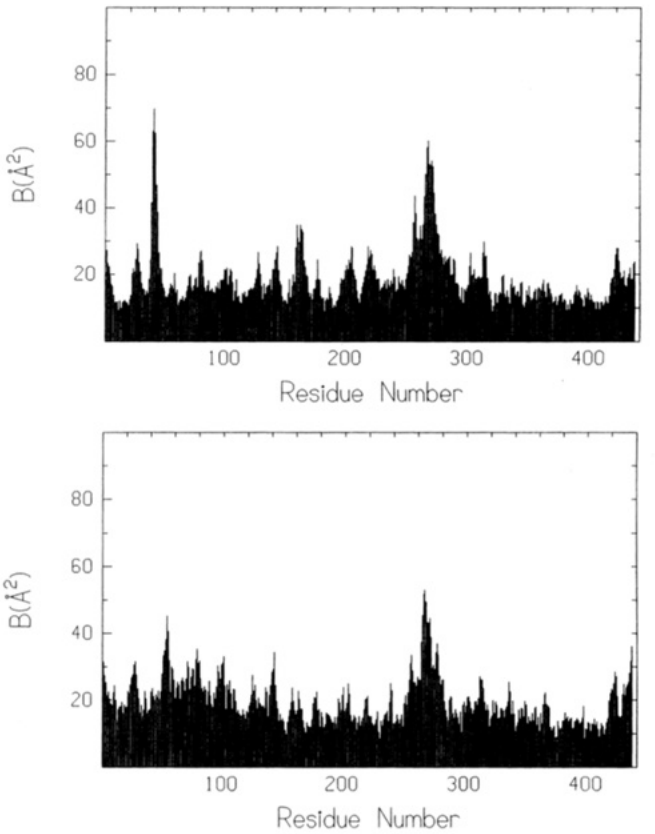

FIGURE 3: Mean main-chain temperature factor *vs* amino acid residue for (a, top panel) subunit I of the Mg^{II}-enolase complex and (b, bottom panel) subunit I of the enolase−$(Mg^{II})_2$−PhAH complex (PDB entry 1EBG). (Weighted averages for the open and closed forms of the active site loop were considered for the Mg^{II}-enolase complex.)

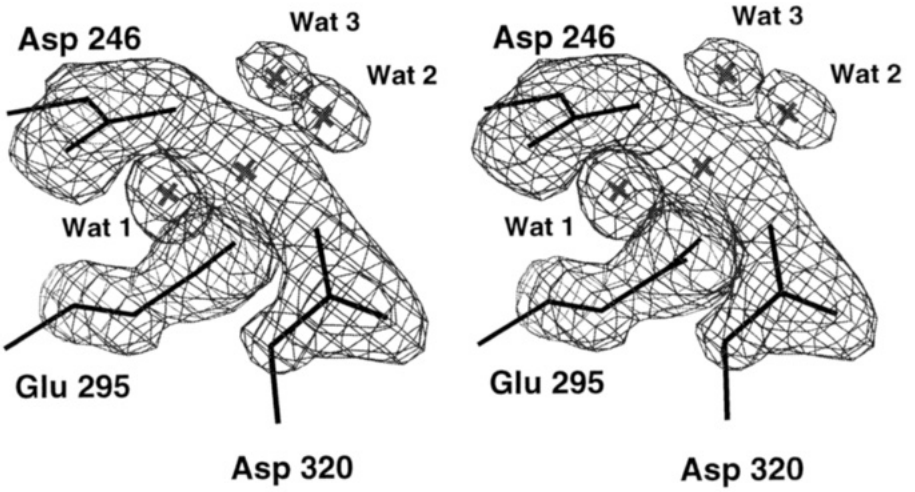

FIGURE 4: Representative F_o-F_c electron density map calculated with the final refined phases and contoured at 2σ. The metal, waters, and protein metal ligands (subunit II) beyond the α carbon were excluded. Ligands Asp 246, Asp 320, and Glu 295 and waters 1 through 3 are indicated. Because the electron density map was calculated on the same scale as that in Figure 2, the noise level of the latter map was used to compute the σ value of 2 reported.

multiple conformations previously (Zhang et al., 1994), the closed conformation reported here (denoted by the letter *C* in the PDB file) is most comparable to the model of Wedekind et al. (1994). Mobile elements are similar to those previously reported for the apo, holo, and substrate-bound structures (Stec & Lebioda, 1990; Lebioda & Stec, 1989, 1991). Representative mean main-chain temperature factors for subunit I of the Mg^{II}-enolase complex are shown in Figure 3a (top panel). The average overall protein temperature factor is 21 Å^2 for the Mg^{II}-enolase dimer. The α carbons of the independently modeled enolase subunits superimpose with an rms deviation of 0.14 Å despite the asymmetry imposed by the crystal packing environment.

The absence of substantial changes in the tertiary and quaternary fold of the Mg^{II}-enolase complex, compared to its companion structures obtained from low pH and high ionic strength, validates a superposition analysis described in a previous study (Wedekind et al., 1994). This analysis concluded that the conformational changes of the enolase−$(Mg^{II})_2$ − PhAH complex were not due to the change of space group and crystallization conditions, but instead were the result of inhibitor binding. To emphasize the latter point, the main-chain temperature factors of the Mg^{II}-enolase and enolase−$(Mg^{II})_2$ − PhAH complexes are shown in Figure 3. Both structures were obtained from virtually identical crystallization conditions, however the PhAH-bound enzyme generally exhibits lower temperature factors (Figure 3b, bottom panel) in regions that correlate directly with an association of the enzyme structure and the inhibitor as mediated by ionic or hydrogen bonding interactions (Wedekind et al., 1994).

Metal Coordination. The coordination sphere of Mg^{2+} at the metal **I** site has not been determined previously for the substrate- or inhibitor-free enzyme. Several reported structures of enolase describe a trigonal bipyramidal geometry for metal **I** in the presence of "activating" metals. In these structures, the protein ligands and either one (Lebioda & Stec, 1991; Lebioda et al., 1991, 1993) or two waters (Lebioda & Stec, 1989) complete the metal coordination sphere. The possible mechanistic significance of trigonal bipyramidal geometry has been discussed extensively (Lebioda & Stec, 1989, 1991; Gerlt et al., 1991; Cleland, 1992; Poyner & Reed, 1992).

Figure 4 shows $F_o - F_c$ electron density calculated from a refined model in which Mg^{2+}, the coordinating waters, and the ligand side chains of residues 246, 295, and 320 were omitted prior to refinement and generation of the electron density map. Adjacent water ligands are approximately 2.8 Å apart. The average Mg^{II}−oxygen distance for all six ligands is 2.1 Å. The resulting octahedron is slightly distorted in the plane composed of waters 1 through 3 and Glu 295 (Figure 4). Interaxial angles in this plane range from 74° to 102°. The average temperature factor for coordinating waters is 20 Å^2, whereas the average Mg^{2+} temperature factor is 14 Å^2. Water 1 of the octahedron is trapped between Oδ2 of Asp 246, Oδ2 of Glu 296, and the Mg^{2+} ion. All structures of enolase with bound metal ions maintain this interaction with water 1. Displacement of this water cannot be achieved easily without loss of metal **I** or movement of residue 296. Water 2 makes direct hydrogen bond contacts to the side chains of Lys 396 and Glu 168 in addition to neighboring waters in the active site. Water 3 interacts directly with the amide side chain of Gln 167. The higher pH and lower ionic strength of the crystallization medium, relative to previous structures obtained from ammonium sulfate at pH 6, most likely account for the tight binding of Mg^{2+} and the localization of three coordinated waters.

Other β-Barrels. MLE (Goldman et al., 1987), CMLE (Hoier et al., 1994), and MR (Neidhart et al., 1991) fold as $\beta_8\alpha_7$-barrels. Similarities among these enzymes have been documented (Neidhardt et al., 1990; Petsko et al., 1993; Hoier et al., 1994). In contrast, enolase is a $\beta\beta\alpha\alpha(\beta\alpha)_6$-barrel although a topological similarity to MLE has been noted (Lebioda & Stec, 1988; Lebioda et al., 1989). Despite differences in connectivity and reactions catalyzed, enolase, MLE, CMLE, and MR have similar N-terminal and C-terminal domain architectures and most likely proceed through a common carbanion intermediate (Petsko et al., 1993; Hoier et al., 1994; Dinovo & Boyer, 1971; Stubbe & Abeles, 1980; Anderson & Cleland, 1990). Superimposition of the three $\beta_8\alpha_7$ structures upon the equivalent $\beta\beta\alpha\alpha(\beta\alpha)_6$ domain of enolase results in a conserved five-stranded core (Figure 5a, top panels). Residues for the alignment were chosen to maintain an optimal match among spatially conserved metal ligands, and the parallel sheet of the barrel

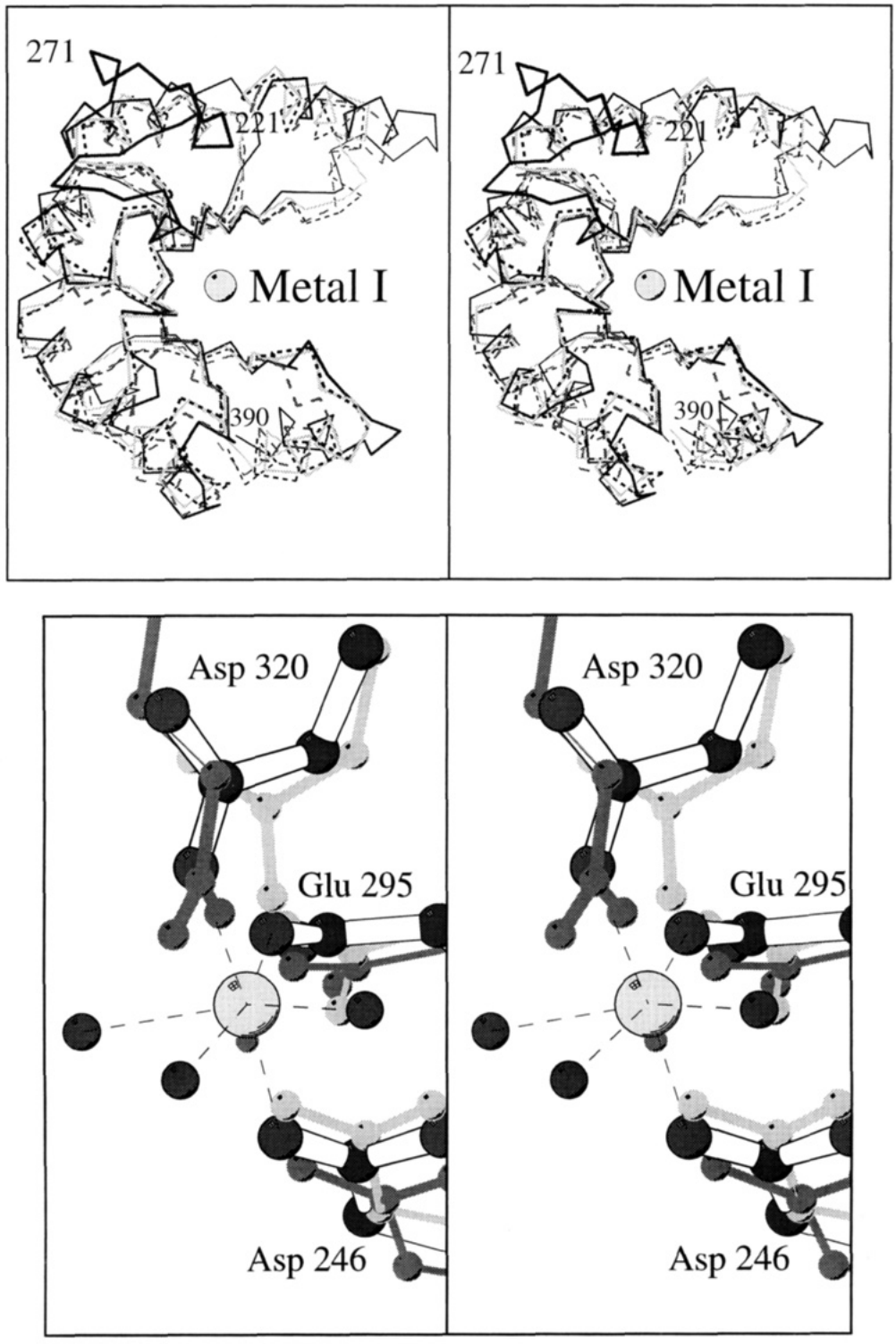

FIGURE 5: Selected α/β-barrel α carbon coordinates for MLE, CMLE, and MR superimposed upon the Mg^{II}-enolase complex (subunit I). A space-filling model of enolase metal **I** has been included. (a, top panels) Global superposition of residues 178−319 of MLE (solid gray line), residues 174−315 of CMLE (short broken line), residues 174−310 of MR (long broken line), and residues 221−390 of enolase (solid black line). The N-terminal domains and strands 1, 2, and 8 of the barrels have been omitted for clarity. (b, bottom panels) Close-up of the metal **I** binding site. Schematized ball-and-stick metal ligands are colored as follows: enolase, black and white; MR, dark gray; CMLE, light gray. Respective superimposed side chains of enolase, MR, and CMLE are Asp 246, Asp 195, and Asp 194; Glu 295, Glu 221, and Glu 220; and Asp 320, Glu 247, and Asp 245. A small dark sphere was included to indicate the metal position of MR. Larger black spheres are waters from enolase. (Entries 1MLE, 1CHR, and 2MNR for MLE, CMLE and MR were retrieved from the PDB.) This figure was generated by MOLSCRIPT (Kraulis, 1991).

core. Least-squares fits of 30 α carbons from the $\beta_8\alpha_7$ enzymes and the Mg^{II}-enolase backbone resulted in rms deviations ranging from 0.9 to 1.1 Å. The loop containing residue 271 of enolase (Figure 5a) appears to be the only significantly mismatched region of the alignment. The resulting superposition reveals a conserved metal binding motif (Figure 5b, bottom panels) which may be critical in the ionization of the respective carbon acid substrates for each enzyme. Details of the non-protein metal ligands are not available for CMLE. In the case of MR, the metal

ligands observed for two independently refined high-resolution structures indicate the metal coordination is octahedral as seen in the Mg^{II}-enolase complex. This geometry is observed in both the inhibitor-free and inhibitor-bound structures (PDB entries 2MNR and 1MNS at 1.9 and 2.0 Å resolution, respectively). MLE also coordinates the oxygen atoms from three carboxylate side chains and three ordered water molecules in the substrate- and inhibitor-free enzyme (Helin and Goldman, private communication).

Substrate Binding. Previous studies have likened the coordination of the (Mg^{II})−PhAH complex of enolase to the binding of the *aci*-carboxylate form of 2-PGA at the active site of enolase following abstraction of the C2 proton (Anderson et al., 1984; Poyner & Reed, 1992; Wedekind et al., 1994). The Mg^{II}-enolase structure presented here agrees with the placement of the non-protein ligands in the enolase−$(Mg^{II})_2$−PhAH structure. The hydroxamate and carbonyl oxygens of PhAH must displace waters 2 and 3, respectively, in the Mg^{II}-enolase coordination sphere (Figure 4). A similar scheme could be envisioned for the alcohol and carboxyl oxygens of 2-PGA in order to stabilize the anionic character of the reaction intermediate (Poyner & Reed, 1992). Similarly, chelation of a metal by the carboxylate and alcohol groups of mandelate has been invoked in the mechanism of MR (Gerlt & Gassman, 1993; Landro et al., 1994). Therefore, the catalytic and metal binding requirements of enolase, MR, CMLE, and MLE in conjunction with the observed octahedral coordination in the Mg^{II}-enolase and enolase−$(Mg^{II})_2$−PhAH complexes (Wedekind et al., 1994) suggest that octahedral geometry is the fundamental coordination motif in each of these enzymes, and that this motif is structurally conserved in both the substrate and catalytic complexes.

ACKNOWLEDGMENT

We thank Dr. Russell R. Poyner for the purified yeast enolase.

REFERENCES

Anderson, V. E. (1981) Ph.D. Dissertation, University of Wisconsin−Madison, Madison, WI.
Anderson, V. E., Weiss, P. M., & Cleland, W. W. (1984) *Biochemistry 23*, 2779−2786.
Brünger, A. T. (1992) X-PLOR version 3.1. *A system for X-ray Crystallography and NMR*, New Haven, CT.
Cardenas, J. M., & Wold, F. (1971) *Arch. Biochem. Biophys. 144*, 663−672.
Castellano, E. E., Oliva, G., & Navaza, J. (1992) *J. Appl. Crystallogr. 25*, 281−284.
CCP4 (1979) *A Suite of Programs for Protein Crystallography*, SERC Daresbury Laboratory, Warrington, England.
Cleland, W. W. (1992) *Biochemistry 31*, 317−319.
Dinovo, E. C., & Boyer, P. D. (1971) *J. Biol. Chem. 246*, 4586−4593.
Faller, L. D., Baroudy, B. M., Johnson, A. M., & Ewall, R. X. (1977) *Biochemistry 16*, 3864−3869.
Fox, G. C., & Holmes, K. C. (1966) *Acta Crystallogr. 20*, 886−891.
Gerlt, J. A., & Gassman, P. G. (1993) *Biochemistry 32*, 11943−11952.
Gerlt, J. A., Kozarich, J. W., Kenyon, G. L., & Gassman, P. G. (1991) *J. Am. Chem. Soc. 113*, 9667−9669.
Goldman, A., Ollis, D. L., & Steitz, T. A. (1987) *J. Mol. Biol. 194*, 143−153.
Hoier, H., Schlömann, M., Hammer, A., Glusker, J. P., Carrell, H. L., Goldman, A., Stezowski, J. J., & Heineman, U. (1994) *Acta Crystallogr., Sect. D50*, 75−84.
Jones, T. A. (1978) *J. Appl. Crystallogr. 11*, 268−276.
Kabsch, W. (1978) *Acta Crystallogr., Sect. A32*, 922−923.
Kabsch, W. (1988a) *J. Appl. Crystallogr. 21*, 67−71.
Kabsch, W. (1988b) *J. Appl. Crystallogr. 21*, 916−924.
Kraulis, P. J. (1991) *J. Appl. Crystallogr. 24*, 946−950.
Landro, J. A., Gerlt, J. A., Kozarich, J. W., Koo, C. W., Shah, V. J., Kenyon, G. L., Neidhart, D. J., Fujita, S., & Petsko, G. A. (1994) *Biochemistry 33*, 635−643.
Lebioda, L., & Brewer, J. (1984) *J. Mol. Biol. 180*, 213−215.
Lebioda, L., & Stec, B. (1988) *Nature 333*, 683−686.
Lebioda, L., & Stec, B. (1989) *J. Am. Chem. Soc. 111*, 8511−8513.
Lebioda, L., & Stec, B. (1991) *Biochemistry 30*, 2817−2822.
Lebioda, L., Stec, B., & Brewer, J. M. (1989) *J. Biol. Chem. 264*, 3685−3693.
Lebioda, L., Stec, B., Brewer, J. M., & Tykarska, E. (1991) *Biochemistry 30*, 2823−2827.
Lebioda, L., Zhang, E., Lewinski, K., & Brewer, J. M. (1993) *Proteins: Struct., Funct. Genet. 16*, 219−225.
Navaza, J. (1987) *Acta Crystallogr., Sect. A43*, 645−653.
Navaza, J. (1990) *Acta Crystallogr., Sect. A46*, 619−620.
Neidhart, D. J., Kenyon, G. L., Gerlt, J. A., & Petsko, G. A. (1990) *Nature 347*, 692−694.
Neidhart, D. J., Howell, P. L., Petsko, G. A., Powers, V. M., Rongshi, L., Kenyon, G. L., & Gerlt, J. A. (1991) *Biochemistry 30*, 9264−9273.
Petsko, G. A., Kenyon, G. L., Gerlt, J. A., Ringe, D., & Kozarich, J. W. (1993) *Trends Biochem. Sci. (Pers. Ed.) 18*, 372−376.
Poyner, R. R., & Reed, G. H. (1992) *Biochemistry 31*, 7166−7173.
Sack, J. S. (1988) *J. Mol. Graphics 6*, 224−225.
Stec, B., & Lebioda, L. (1990) *J. Mol. Biol. 211*, 235−248.
Stubbe, J., & Abeles, R. H. (1980) *Biochemistry 19*, 5505−5512.
Tronrud, D. E., Ten Eyck, L. F., & Matthews, B. W. (1987) *Acta Crystallogr. Sect. A43*, 489−501.
Wedekind, J. E., Poyner, R. R., Reed, G. H., & Rayment, I. (1994) *Biochemistry 33*, 9333−9342.
Wold, F., & Ballou, C. E. (1957) *J. Biol. Chem. 227*, 313−328.
Zhang, E., Hatada, M., Brewer, J. M., & Lebioda, L. (1994) *Biochemistry 33*, 6295−6300.

BI942683Z